Journal of Petroleum Exploration and Production Technology
https://doi.org/10.1007/s13202-020-00935-z

ORIGINAL PAPER-- PRODUCTION ENGINEERING

Alternating N_2 gas injection as a potential technique for enhanced gas recovery and CO_2 storage in consolidated rocks: an experimental study

Nuhu Mohammed[1] · Abubakar Jibrin Abbas[1] · Godpower C. Enyi[1] · Salihu M. Suleiman[1] · Donatus E. Edem[1] · Muhammad Kabir Abba[1]

Received: 21 April 2020 / Accepted: 11 June 2020

Abstract

The promotion of enhanced gas recovery (EGR) and CO_2 storage is still shrouded in contention and is not well accepted, due to the excessive in situ CO_2 mixing with the nascent natural gas. This adulterates the recovered CH_4 and thus results in a high sweetening process cost thereby making the technique impractical. This has not only limited the field application of EGR in actual projects to a few trails but renders it uneconomical. This study aims to present, experimentally, alternating N_2 injection as a potential technique for EGR and CO_2 storage in sandstone rock cores. A laboratory core flooding experiment was carried out to simulate a detailed process of unsteady-state methane (CH_4) displacement using Bandera grey core plug. This was carried out at 40 °C, 1500 psig, and 0.4 ml/min injection rate by alternative injection of N_2 and CO_2 in succession designed to suit the application based on optimum operating conditions. The results show that both CO_2 storage capacity and CH_4 recovery improved significantly when gas alternating gas (GAG) injection was considered. The best results were observed at lower N_2 cushion volumes (1 and 2 PV). Therefore, the GAG injection method with N_2 as cushion gas can potentially increase both CO_2 storage and CH_4 recovery of the gas reservoir. This technique if employed will assert the current position and provide vital information for further researches aimed at promoting environmental sustainability and economic viability of the EGR and CO_2 sequestration processes.

Keywords Dispersion coefficient · Enhanced gas recovery · Cushion gas · Breakthrough · Concentration profile

List of symbols

yCO_2	CO_2 mole fraction
yN_2	N_2 mole fraction
D	Diffusion coefficient, m^2/s
Q	Flow rate mil/min
t_D	Dimensionless time
x_D	Dimensionless distance
d	Characteristic length scale, m
K_L	Longitudinal dispersion, m^2/s
L	Core sample length, mm
L_{exp}	Experimental length, m
μ	Viscosity, cP
P	Pressure, psig
T	Temperature, K
u	Interstitial velocity, m/s
ϕ	Core porosity, %
α	Dispersivity, m
τ	Tortuosity
Pe	Péclet number
Pe_m	Medium Péclet number
PV	Pore volume
r	Radius of core sample, m
λ_{90}	Lambda function at 90% of effluent concentration
λ_{10}	Lambda function at 10% of effluent concentration

Introduction

CO_2 emissions are generalized as a significant factor responsible for inhibiting climate change that later results to increase in environmental temperature (global warming). It was predicted that there will be a rise in world temperature and sea level from 1.9 to 3.5 °C and 18–30 cm, respectively, by the year 2100. These would be accompanied by

Electronic supplementary material The online version of this article (https://doi.org/10.1007/s13202-020-00935-z) contains supplementary material, which is available to authorized users.

✉ Nuhu Mohammed
n.mohammed5@edu.salford.ac.uk

[1] University of Salford, Manchester, UK

Published online: 20 June 2020

many foreseen distresses (Meehl et al. 2005). The effective simultaneous enhanced gas recovery and sequestration using CO_2 injection are losing recognition due to high natural gas contamination, premature breakthrough, and high compression ratio, since it requires about six (6) molar volume of it to displaced one (1) molar volume of natural gas, thereby hindering its market and calorific which eventually render the process non-economically viable. In contrast, N_2 can be recovered mostly from the air separation unit (ASU) or as byproducts of oxygen plants. It requires less compression ratio, which is why a lower amount of it is needed to create high pressure in the CH_4 reservoir.

The increase in carbon credit, coupled with earlier energy demand due to population growth, has forced the exploitation of alternative sources of energy, using other fewer or zero-emission technologies (Abba et al. 2017). Natural gas is considered one of the abundant, low emission, cleanest, and affordable sources of fossil fuels (Benson et al. 2005; Al-Abri et al. 2012). Carbon dioxide (CO_2) underground storage for simultaneous storage and natural gas (CH_4) displacement is gaining attention worldwide (Ganjdanesh and Hosseini 2017; Raza et al. 2017). This underground storage can be in the form of oil and gas conventional reservoirs or deep saline aquifers (Abba et al. 2018). Conventional natural gas reservoirs have the potential to safely store anthropogenic CO_2, due to its proven integrity of gas storing capability (Kalra and Wu 2014). Thus, in turn, issues of CO_2 leakages and contamination of adjacent freshwater aquifers are minimal. This arises the need for the development of other injection techniques capable of enhancing both natural gas recovery and CO_2 storage (Abba et al. 2018).

Tertiary enhanced gas recovery (EGR) and storage by CO_2 injection are gaining recognition within the research environment due to its greenhouse gases (GHGs) reduction potential. Therefore, both nitrogen (N_2) and CO_2 can be used to increase nascent HCs yield from oil and gas reservoirs. However, CO_2 drawbacks are mainly excessive mixing and high compression ratio, thus hindering the overall process uneconomically viable. In contrast, N_2 can be recovered virtually from the atmospheric air, through air separation units. It requires less compression ratio than CO_2, which is why a lower amount of it was needed to create high pressure in the CH_4 reservoir.

The promotion of EGR is still at its infant stage due, to the excessive mixing between the injected (displacing fluid) CO_2 and the nascent displaced fluid (natural gas) during the flooding process (Oldenburg and Benson 2002; Shtepani 2006; Turta et al. 2007; Sim et al. 2008, 2009; Al-abri et al. 2009; Sidiq et al. 2011; Hughes et al. 2012; Honari et al. 2013, 2015, 2016; Khan et al. 2013; Zhang et al. 2014; Patel et al 2016). This adulterates the recovered natural gas and thus reduces its heating and market value, which results in the high cost of the sweetening process to maintain its market value (Oldenburg and Benson 2002; Sim et al. 2009). This has not only limited the EGR project to a few pilot trials (Pooladi-Darvish et al. 2008) but also made the process apparently uneconomical due to unprecedented mixing with the displaced gas, which make the phenomenon to be poorly understood (Patel et al. 2016). Thus, finding a suitable technique for reducing such in situ mixing could be valuable at first by injecting a certain amount of nitrogen gas as cushion gas before the invention of CO_2, which is the concept behind gas alternating gas injection.

Several authors (Xidong et al. 2019; Hughes et al. 2012; Janssen et al. 2018; Abba et al. 2018) have carried out an extensive study on how to delay CO_2 breakthrough time during EGR process. Among them, Abba et al. (2018) and Xidong et al. (2019) were able to achieve reasonable improvement. Abba et al., (2018) use varying connate water concentration and was able to delay CO_2 breakthrough by 20 min at a concentration of 10 wt.% sodium chloride (NaCl). On the other hand, Gu et al. (2019) use different mole ratios of CO_2/N_2 mixture gases in coalbed core samples. They reveal that injection of N_2-rich mixtures contributes to preventing the nascent early breakthrough of injected CO_2 and safely stored large volumes of CO_2 into the shale sediment over the long term. Abba et al. (2019) achieved a high percentage of total CO_2 injected stored at 10 wt.% salinity using solubility trapping mechanism, but with least CH_4 recovery resulted from the density of connate water sealing off the narrow pore spaces within the pore matrix.

To our knowledge, no established efficient method capable of improving simultaneous natural gas recovery and CO_2 storage has been highlighted. This necessitated the need for an in-depth study to develop novel approaches and ways to minimizing this complex phenomenon of gas mixing during gas–gas displacements since the two gases (CO_2 and CH_4) are miscible in all outcomes (Abba et al. 2018). This study aims to highlight, experimentally, the potential of using N_2 as cushion gas in a novel gas alternating gas (GAG) technique to reduce or minimize excessive mixing during EGR by CO_2 injection, thereby improving CH_4 recovery while subsequently storing substantial volumes of CO_2 in conventional natural gas reservoirs.

Dispersion theory and equation

The term Péclet number, Pe, is a dimensionless measure of the level of dispersion by a solute which is defined as the ratio of advective to dispersive processes (Rose 1973) as reported by (Ho and Webb 2006). The degree or level of dispersion is inversely proportional to the magnitude of the Péclet number. At low Péclet numbers, the degree of dispersion is large. It is expressed as in Eq. (1).

$$P_e = \frac{uL}{K_l} \tag{1}$$

Péclet number (ratio of convection to dispersion), L is the core sample length.

In 1963, Perkins and Johnston denoted different termed to Péclet number called medium Péclet number (Pe_m). Its value generally determined and describes the dominant displacement fluid region as the dispersion process progresses shown in Eq. (2):

$$Pe_m = \frac{ud}{D} \tag{2}$$

where Pe_m is medium Péclet number, $u =$ is the mean interstitial velocity (m/s), D is the diffusion coefficient (m^2/s), and d is the porous medium characteristic length scale, termed as the medium-grain diameter of the sand pack, but it is poorly defined in consolidated medium (Hughes et al. 2012).

Ideally when $Pe_m < 0.1$ diffusion becomes dominants, while advective mixing dominates the dispersion process at higher medium Péclet number i.e. at $Pe_m > 10$.

Delgado, in 2001, uses the Lambda function, by plotting a graph of Lambda at different experimental times against the percent of displacing fluid in an arithmetic probability paper. The dispersion coefficient was then evaluated using Eq. (3).

$$K_L = u \times L\left(\frac{\lambda_{90} - \lambda_{10}}{3.625}\right)^2 \tag{3}$$

where $K_L =$ longitudinal dispersion coefficient (m^2/s), $u = \frac{Q}{\pi r^2 \phi}$ is the average interstitial velocity (m/s), and ϕ is the porosity, $L =$ length of porous media (m), λ_{90} and $\lambda_{10} =$ are values of Lambda function at 10 and 90% effluent concentration. In this research, the lambda function techniques were used, as the fundamental equation was derived by considering inert gas (N_2) as one of the displacing fluids.

Diffusion theory and equation

The diffusion coefficient (D) signifies the extent or magnitude at which a substance or fluid disperses through a unit area (m^2) per unit time (s) at a given or defined unit concentration gradient. The proposed empirical model which relates the molecular diffusion, temperature, and pressure for empirical diffusion coefficient determination as revealed by (Hughes et al. 2012; Liu et al. 2015) was developed by Takahashi and Iwasaki in 1970. Also, this empirical equation has been tested by various researchers in determining the real and accurate diffusivity using Eq. (4) at conditions applicable to EGR by CO_2 injection. The diffusion coefficient of CO_2 in CH_4 was dignified at 298–348 K and pressures of 5–15 MPa in a porous bronze plug (Takahashi and Iwasaki 1970). The results were well within the range of conditions applicable to EGR (Abba et al. 2017).

$$D_{CO_2,CH_4} = \frac{\left(-4.3844 \times 10^{-13} P + 8.5440 \times 10^{-11}\right) T^{1.75}}{P} \tag{4}$$

where D_{CO_2,CH_4} is the molecular diffusion coefficient of CO_2 in pure CH_4 calculated in $m^2\ s^{-1}$ with P in MPa and T in K. The absolute average deviation (AAD) of this correlation from the experimental data was 1.5% over the range of 298–348 K and 5–15 MPa (Abba et al. 2017, 2018). In this study, a different model was used to cater for the inclusion of nitrogen (N_2) gas during the natural gas displacement and CO_2 sequestration. This model equation is presented in Eq. 5. A correlation formula obtained by Fuller et al. (1966) by means of computer-aided correlation of 340 experimental points is expressed as:

$$D_{N_2,CH_4} = \frac{1.0110 \times 10^{-4} T^{1.75} \sqrt{\left(1/\mu_{N_2} + 1/\mu_{CH_4}\right)}}{P\left[\left(\sum V_{N_2}\right)^{1/3} + \left(\sum V_{CH_4}\right)^{1/3}\right]^2} \tag{5}$$

where $(\sum V_{N_2})$ and $(\sum V_{CH_4})$ are the values derived from the summation of atomic diffusion volumes of N_2 and CH_4 molecules, respectively. These values and other simple molecules are presented in Table 1.

The equation was further simplified after inserting the values of atomic diffusion volumes and the molecular weight of nitrogen and methane. The same was applied for carbon dioxide and methane displacement mechanism. These simplified equations are presented in Eqs. (6) and (7)

$$D_{N_2,CH_4} = \frac{10.2 \times 10^{-11} T^{1.75}}{P} \tag{6}$$

$$D_{CO_2,CH_4} = \frac{8.2 \times 10^{-11} T^{1.75}}{P} \tag{7}$$

where T and P are temperatures and pressure in Kelvin (K) and megapascal (MPa), respectively. For example, at the same temperature and pressure, Eq. (7) was validated using the experimental work of Abba et al, 2018. The molecular diffusion coefficient (D_{CO_2,CH_4}) was found to be 22.52×10^{-8} m^2/s. This value is 0.18% in absolute average deviation (AAD) when compared with Abba et al. (2018) findings.

Materials description

In this research, an experimental study approach using the core flooding system was investigated. This entitles saturating the core plug with CH_4 and the injection of CO_2 at different N_2 gas cushion volumes. The core plug use was Bandera grey sandstone as presented in Table 2.

Table 1 Atomic diffusion contributions for various gas element and molecules

S/N	Molecule	Diffusion volume
1	He	2.67
2	Ne	5.98
3	Ar	16.2
4	Kr	24.5
5	Xe	32.7
6	H_2	6.12
7	D_2	6.84
8	N_2	18.5
9	O_2	16.3
10	Air	19.7
11	CO	18.0
12	CO_2	26.9
13	N_2O	35.9
14	NH_3	20.7
15	H_2O	13.1
16	SF_6	71.3
17	Cl_2	38.4
18	Br_2	69.0
19	SO_2	41.8
20	C	15.9
21	H	2.31
22	O	6.11
23	N	4.54
24	F	14.7
25	Cl	21.0
26	Br	21.9
27	I	29.8
28	S	22.9

Source: Fuller et al. (1966)

Table 2 Dimensions and petrophysical properties of Bandera grey core sample

Core sample	Length (mm)	Diameter (mm)	Porosity (%)	Gas Permeability (md)	Gas in Place (PV)
Bandera grey	76.02	25.31	19.68	32	115

Materials

The core plug of dimension 1.0 inch diameter and 3.0 inch length was used as present in Table 2. This sandstone is considered a classic sedimentary rock primarily comprised of quartz, silica, and sand-sized minerals. For consistency, the porosity and permeability of the sandstone core samples were determined and compared with the ones provided by the supplier (Kocurek Industries INC, Hard Rock Division, 8535 State Highway 36 S Caldwell, TX 77836, Texas USA). The research-grade CO_2, N_2, and CH_4 with a purity greater than 99.99% were sourced from BOC UK.

Experimental method

A sequence of experimental tests was carried out to investigate the potential of N_2 as cushion gas for enhanced CH_4 recovery and CO_2 storage during core flooding experiment with Bandera grey core plug as the porous medium. Prior to the experiment, the core plug petrophysical properties were evaluated to endured are in synergy with the ones from the vendor. The flow behaviour of supercritical N_2, CO_2, and N_2–CO_2–CH_4 interplay was studied using FLUIDAT^R thermodynamic software. This was vital, in understanding the flow behaviour of supercritical CO_2 as it plumes transverses the pore spaces within the porous medium while displacing the nascent CH_4, especially with the N_2 as cushion gas. Followed to that, a laboratory core flooding experiment was conducted on the Bandera grey core plug to determine the dispersion coefficient, CH_4 recovery, and percent of the CO_2 injected stored of the system at different CO_2 injections and N_2 cushion volumes. Further to that, several runs were carried out at four different N_2 cushion volumes at varying CO_2 injection rates. The effluent stream rates from the core plug were recorded by the two (low and high) gas flow meters. After this, the produced gas compositions are analysed using the Agilent technologies 7890 A model gas chromatography (GC) system at an interval of 5 min elusion time through the sampling valve. The combined data are used to evaluate: one, dispersion coefficient; two, CH_4 recovery; and three; percent of total CO_2 injected stored at the test reservoir conditions of 1500 psig pressure and 40 °C temperature.

Apparatus and procedure

Apparatus

The experimental set-up consists of mainly two individual units; a core lab UFS-200 core flooding system with inbuilt Smart Flood software and packed column design Agilent 7890A gas chromatography (GC) machine model. The core flooding system, designed for 2-phase liquid/gas steady or unsteady state condition displacements, was reconfigured to accommodate additional N_2 as used in the gas alternating gas injection for this study. The integrated online concentration measurement of core flooding effluents was achieved using the GC machine. These values were used in plotting the injection fluids concentration profile as the experiment progress with time. A schematic of the equipment set-up is presented in Fig. 1.

The UFS-200 core flooding system is rated to 5000 and 3750 psig overburden and pore pressure, respectively. The

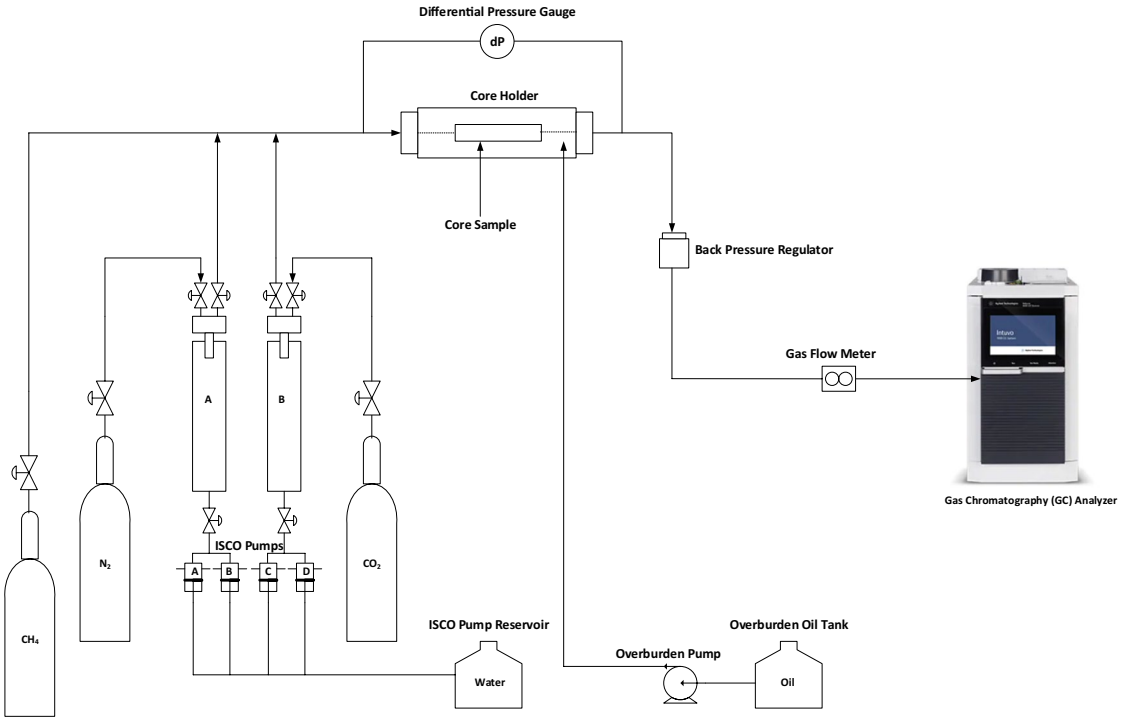

Fig. 1 Schematics of experimentational set-up for gas alternating gas injection

injection system of the equipment is made up of a pair of dual ISCO two-barrel metering pump system (A/B and C/D) for constant flow for pulseless transition and to maintain an accurate flow rate range of 0 to 200 ml/min with a maximum pressure rating of 3750 psig. The pumps are attached to a pair of two stainless-steel floating piston accumulators which are also rated for 5000 psig working pressure and temperature of 177 °C. They are designed for injection of the fluids of interest and can withstand up to 7500 psig test pressure. The hydraulic pump with a maximum of 10,000 psig pressure output was used to set the overburden confining pressure. The Smart Flood 1.0 software forms an essential unit of the system which interfaces the UFS system and the computer data-acquisition-control (DAC) system hardware and generates on-screen automatic logging of test data for all measured values like pressures, temperatures, volumes, etc., to a computer data file. A Rosemount Static DP transmitter with an accuracy of 0.0055% was responsible for measuring the differential pressures across the entire Hassler-type core holder, which was used to house the core sample. The core sample is clutch inside the core holder by a Viton rubber sleeve. A core holder heat jacket to simulate the required temperature was also employed with an accuracy of 0.1%. Dome type back pressure regulator integrated into the flooding system ensured the confinement of the desired pressures within the core holder. Such desired pressure was set using the N_2 cylinder bottle. The effluents from the back-pressure regulator pass through the mass flow controllers that measure the volume of the actual effluents produced before been analysed by the GC system in place.

Procedure

The core sample was dried overnight in an oven at 105 °C for moisture removal and other volatile compounds. The dried sample was wrapped with cling film and in foil paper before inserted into a heat shrink. This is vital to avoid viscous fingering and the penetration of the gases through the sleeve into the ring-shaped core holder. It was then loaded into the core holder and staple with clamps from both ends. Hydraulic oil was then pumped into the ring-shaped core holder to provide the desired overburden pressure, which was kept 500 psig above the pore pressures to in other to avoid fracturing of the core sleeve. The heat jacket was then installed on the core holder and the temperature step-up was observed. The backpressure was engaged and CH_4 was slowly injected into the core sample from the CH_4 cylinder to saturate the core plug until the GC constantly read methane > 99%. N_2 is then injected as cushion gas for about 20 min (1 PV) before the invention of CO_2 at 0.4 ml/min injection rate. Further runs were carried out at increasing N_2 cushion volumes. The experiment elapsed when the methane concentration was insignificant from the GC reading or the CO_2 concentration was > 99%. At each injection time of the GC, the time was noted and the effluent composition which is then used to evaluate the dispersion coefficient, CH_4 recovery,

and percent of total CO_2 injected stored was recorded. The investigation was carried out at 1500 psig pressure and 40 °C temperature. This condition was chosen based on a normal gas pressure reservoir with a gradient of 0.451 psi/ft, an average reservoir depth of 1 km, and a geothermal temperature of 35–40 °C/km. The core sample was dried overnight in an oven at 105 °C for moisture removal and other volatile compounds. The dried sample was wrapped with cling film and in foil paper before inserted into a heat shrink.

Results and discussion

Flow behaviour of supercritical N_2, CO_2, and N_2–CO_2–CH_4 during simulated EGR

The actual flow behaviour of supercritical CO_2 as it plumes traverses the pore spaces within the core sample to displace the in situ methane is quite complex, especially with the inclusion of inert nitrogen gas. Investigating these complexities of displacing fluids (CO_2 and N_2) with regard to the nascent CH_4 is vital in understanding the trends and expected outcomes of the displacement process knowing that these gases in their supercritical state have unique behaviour by exhibiting the density of a liquid but retain the viscosity of a gas (Abba et al. 2018). CO_2 is 2–6 times denser than methane at all relevant reservoir conditions. Besides, CO_2 had a lower mobility ratio compared to methane; thus, it was considered as a high viscosity component (Al-Hasami et al. 2005). Due to the favourability of these properties, CO_2 would be migrated downwards, and this relatively would stabilize the displacement process between the injected CO_2 and methane initially in place (Oldenburg and Benson 2002). The supercritical conditions of CO_2, N_2, and CH_4 are (31.05 °C and 73.80 bar), (− 146.9 °C and 33.90 bar), and (− 82.55 °C and 46 bar), respectively. The experimental conditions employed in this study are well above that of the supercritical temperature and pressure of each single species. The fluids exhibit excellent behaviour due to the response on their transport properties to change from ambient standard conditions to that of EGR condition. A simulation of their respective properties at elevated operational conditions was carried out using FLUIDAT^R software to check the effects of temperature and pressure on the individual gas densities and viscosities at the stated conditions as presented in Fig. 2, 3, and 4. There are pronounced differences in their properties, with CO_2 being much higher and more extreme than those of N_2 and CH_4. The density was said to increase as the gas pressure increases. This was more significant with CO_2 especially at 500–1400 psig range, after which become constant as shown in Fig. 2. This makes CO_2 approximately six (6) times denser than N_2 or CH_4, which signifies the possibility of storing more of it at a supercritical state. However, N_2 and CH_4 exhibited similar behavioural trends as the pore pressure raises, justifying why the recovered CH_4 onsite mostly contain higher traces of N_2 than CO_2 during exploration (Xidong et al. 2019). The kinetic energy of a gas is proportional to its temperature due to the increased rate of collision with the container wall. The reverse was the case to that of liquid fluids due to high inter-molecular forces keeping them close to each other. In general, gas viscosity increases with pressure raise. However, at higher pressures (1300–2000) psig CO_2 maintained high viscosity with a density like that of liquid as observed in Figs. 2 and 3. Also, at

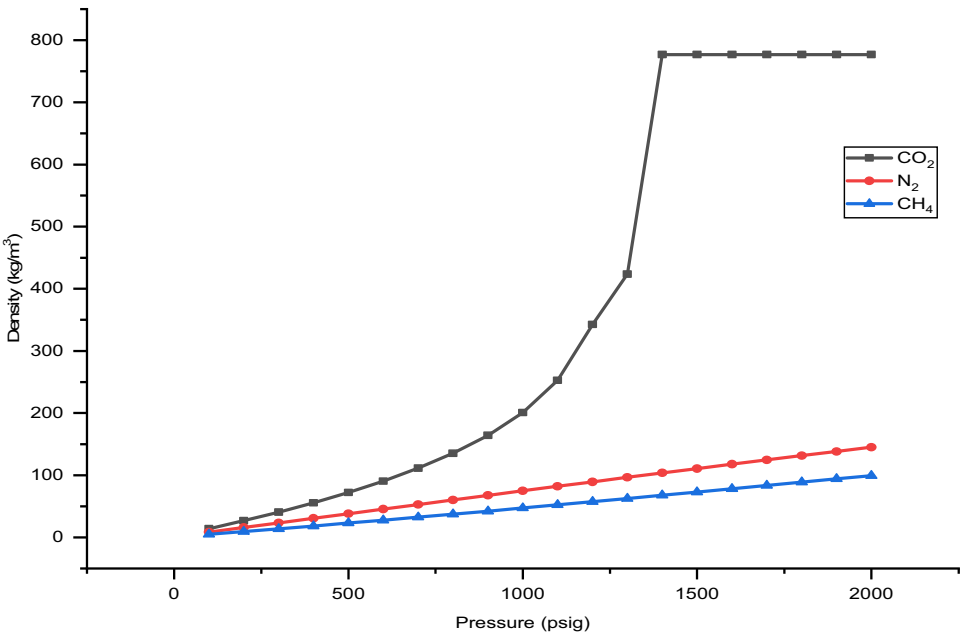

Fig. 2 CH_4, N_2 and CO_2 densities as a function of pressure at 40 °C (generated from FLUIDATR)

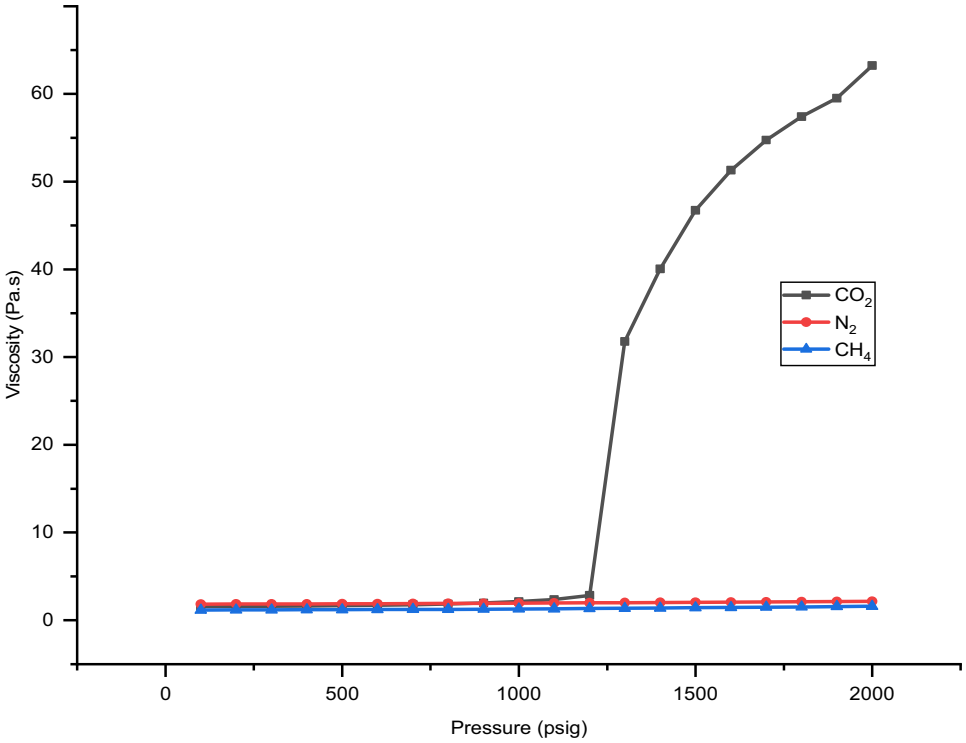

Fig. 3 CH_4, N_2 and CO_2 viscosity as a function of pressure at 40 °C (generated from FLUIDATR)

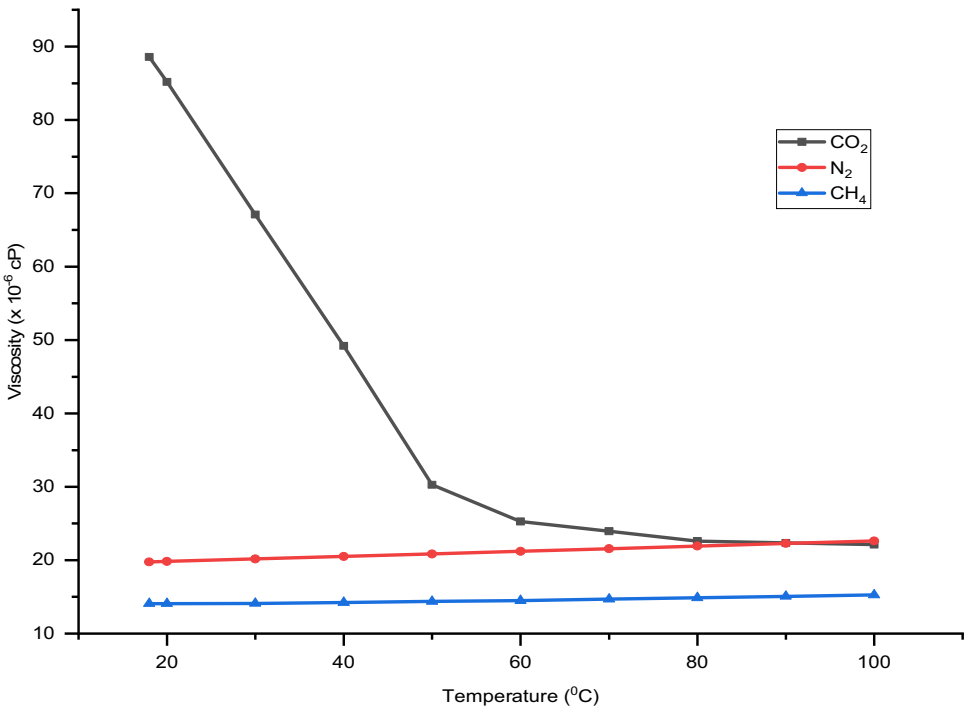

Fig. 4 CH_4, N_2 and CO_2 viscosity as a temperature at 1500 psig (generated from FLUIDAT^R)

a lower temperature (18–50) °C CO_2 experienced viscosity reduction similar to liquid as evidence of an about 66% reduction in viscosity at 50 °C, shown in Fig. 4. Thus, in turn, based on the proceeding statement, CO_2 demonstrated strange properties behaviour compared to those of N_2 and CH_4 at conditions of temperature and pressure (40 °C and 1500 psig) applicable to EGR. This justifies the selection of the experimental conditions as also, reported by Abba et al. 2018. Thus, it makes the application of supercritical CO_2 for the EGR process to be well accepted globally. Such unique esteem property will grossly affect the flow behaviour of the gases as will be presented in the successive sections.

The viscosity is said to be increasing at the beginning of the displacement process until the mobility of the displacing phase is less than that of the displaced phase; this makes the mobility ratio to be less than one (unity). Such a state does maximize gas recovery and sweeps efficiency, due to negligible premature mixing, by providing a sharp viscosity gradient at the displacement front without experiencing viscous fingering effect. A condition in which a combination of two fluids escape some part of the reservoir as it progresses along, forming irregular, or fingered profile. Fingering is relatively a routine problem in reservoirs with gas-injection wells (Al-Abri et al. 2012). Fingering effects result mostly in an unproductive sweeping action, which bypasses many recoverable gas volumes, with a premature breakthrough of displacing fluids. In Fig. 5, both the N_2 injection (CH_4–N_2) and CO_2 injection (CH_4–CO_2) display a lower mobility ratio at their respective critical conditions. The mobility ratio of CH_4–N_2 displacement was low compared to CH_4–CO_2 at pressure (100–800 psig) below CO_2 critical points (33.9 °C and 1070 psig). This means the effect of viscous fingering was minimal as the N_2 plume transverse through the core spaces as against that of CO_2. The effect of pressure on the CH_4–CO_2 mobility ratio was insignificance above its supercritical state and remains almost constant thereafter. Overall, the supercritical state of gases plays an important role in investigating their flow behaviour with maximum recovery efficiency, creating an even flood front with minimum risk to viscous fingering effect.

On the other hand, the mobility of CH_4–CO_2 displacement was ascending as the temperature increase due to an increase in density with temperature and pressure down the reservoir. However, a reverse scenario was observed for that of the CH_4–N_2 process as the temperature increases to 100 °C as observed in Fig. 6. This is so because as the temperature increases CH_4–N_2 system experienced a high rise in diffusion coefficient compared to those of CH_4–CO_2 and CO_2–N_2 as shown later in Fig. 7. Thus, in turn, CH_4–CO_2 system mobility is more sensitive to change in temperature and pressure compared to that of CH_4–N_2 during EGR and storage.

The developed Eqs. (6), (7) derived from the fundamental (first principle) correlation [Eq. (5)] as reported by Fuller et al. (1966) were used to simulate the effect of pressure and temperature for N_2–CH_4, CO_2–CH_4, and CO_2–N_2 interaction behaviours. This simulation was carried out at constant temperatures of 30, 40, and 50 °C, respectively, at a varying pressure of 100–2000 psig for the stated interactions. In Fig. 7, the molecular diffusion coefficient increases with a roughly constant value of 1.5 m^2/s at constant temperatures of 30, 40, and 50 °C over the pressure ranges. These values were more pronounced for CH_4–N_2 interaction than that of CH_4–CO_2 due to the high density and molecular weight of carbon dioxide compared to that of nitrogen at reservoir condition. Meanwhile, above 1500 psig of pressure, the diffusion coefficient trend was the same for all the temperatures and the decline rate was less notable.

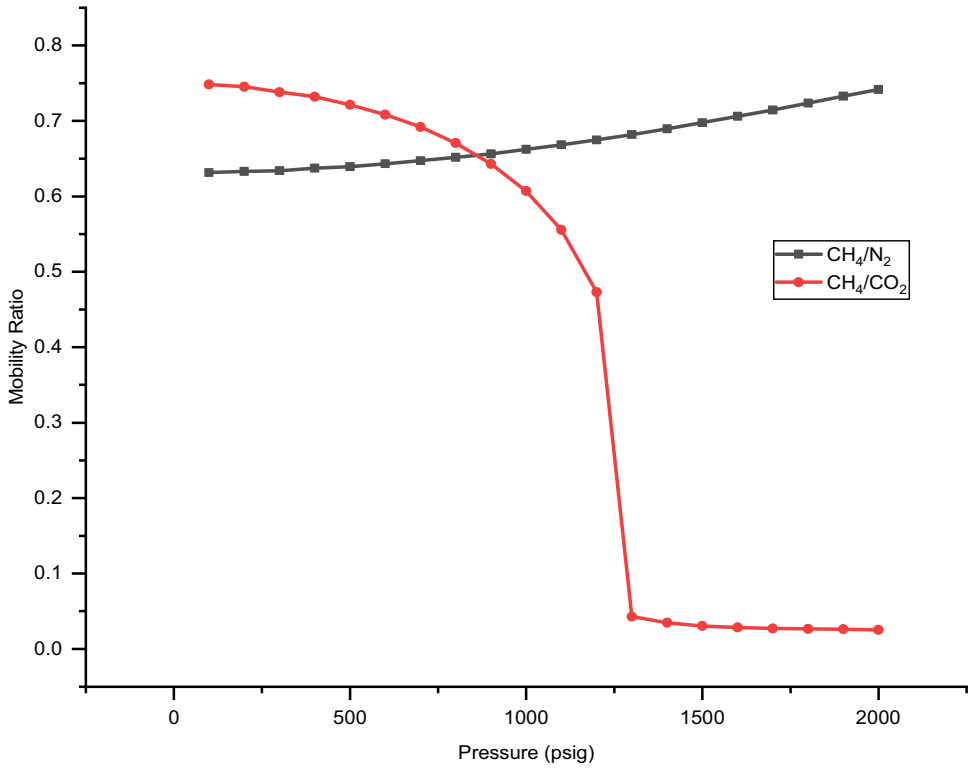

Fig. 5 CH_4–N_2 and CH_4–CO_2 mobility ratios as a function of pressure at 40 °C

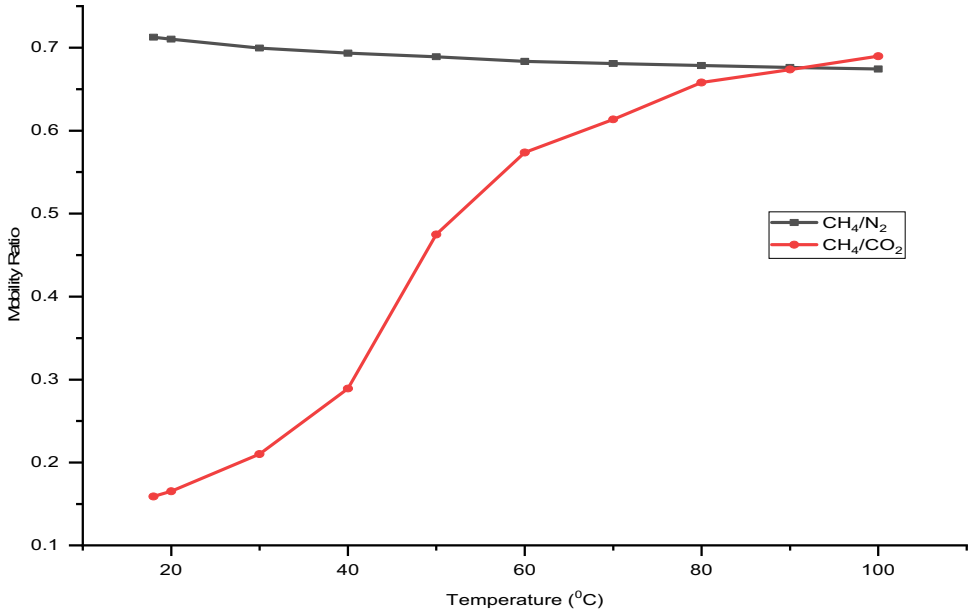

Fig. 6 CH_4–N_2 and CH_4–CO_2 mobility ratios as a function of temperature at 1500 psig

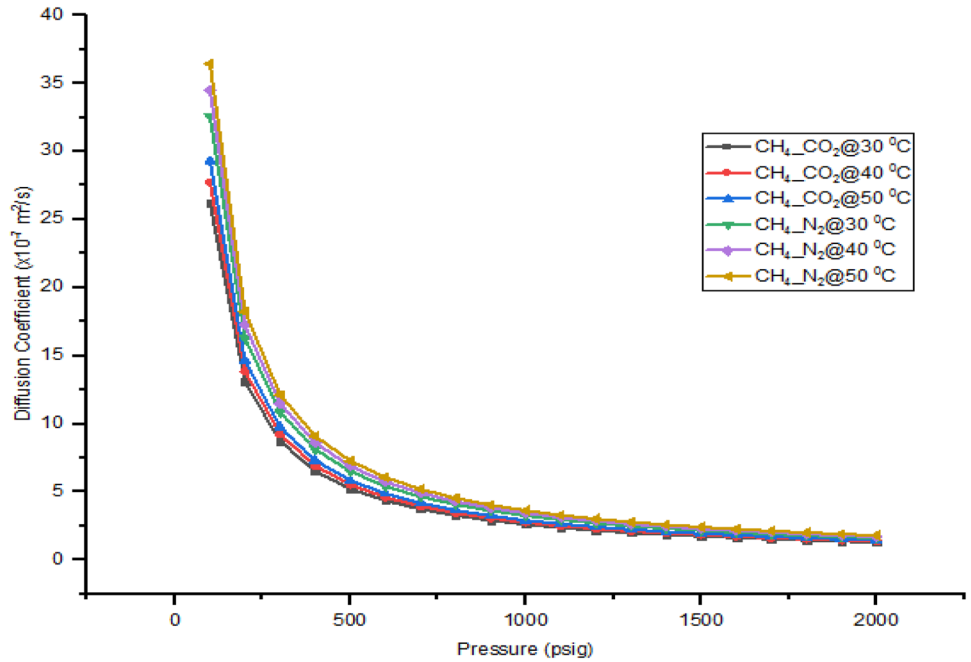

Fig. 7 Effect of pressure on diffusion coefficients for CH_4–N_2 and CH_4–CO_2 interaction at constant temperature of 30, 40, and 50 °C

Temperature plays a significant role in determining the extent of diffusion when two fluids are in contact with each other especially of the same phase. The higher the temperature, the more the kinetic energy due to high collision velocity, which invariably results in the high molecular diffusion coefficient. Such evidence can be seen in Eqs. (6), (7) with the temperature component (in Kelvin) being the rise to the order of 1.75. Viscosities and atomic diffusion also contribute to measuring the overall diffusion coefficient of binary mixtures. Further to that, atoms or molecules with higher viscosities and diffusion volumes do result in lower molecular diffusion coefficient value compared to those with lower viscosities and diffusion volumes, respectively. Figure 8 presents a plot of diffusion coefficient against temperature. The CH_4–N_2 binary mixture shows a high periodic increase as the temperature rise to 120 °C (393.15 K). However, a lower rise was experienced for the case of the CH_4–CO_2 mixture. This was due to high density, viscosity, and diffusion volume of CO_2 at the supercritical condition as against that of N_2. Also, a similar trend was observed for that of the CO_2–N_2 binary mixture.

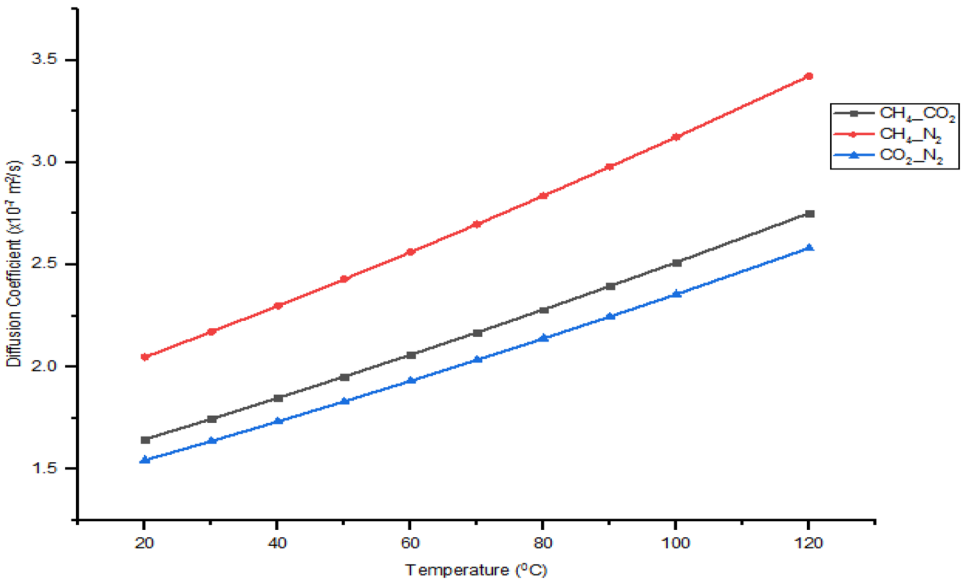

Fig.8 Effect of temperature on diffusion coefficients for CH_4–N_2, CH_4–CO_2, and CO_2–N_2 interaction at constant pressure of 1500 psig

Core flooding experiment

The recovery efficiency and percent of total CO_2 injected stored were analysed by a laboratory displacement system of an experiment to evaluate the concentration profiles of the interacting gases. This involved the injection of N_2 and CO_2 into the Bandera grey core plug at a condition reasonable for the EGR process.

The concept of N_2 as a cushion gas during enhanced gas recovery

The principle behind the whole concept of the core flooding experiment for CH_4 displacement in a porous medium is well understood using the concept of dispersion theory and its governing equations. For example, establishing the dominant mechanism of displacement as the displacing gases (N_2 and CO_2) transverses the core samples are prerequisites to avoid excessive mixing during the EGR process. If the medium Péclet number in Eq. (2) is less than 0.1, diffusion dominates and the flow is driven by the concentration gradient, and the transport is influenced by the mobility ratio, as evident in most of the experimental EGR process. However, when the Péclet number is above 10 advective mixing dominates due to the turbulence and eddy current effects and the flow is driven by velocity gradient as seen in most displacement at higher injection velocity. In this experiment, the Péclet number was 0.02, meaning the dominant displacement is by diffusion. The rate of gas miscibility during the natural gas displacement process mostly depends on the injection rate of the displacing species. The higher the rate the more mixing will be recorded, and invariably more contaminated CH_4 will be recorded. This was why most researches on CO_2 injections were tailored toward storage rather than CH_4 recovery. The injected amount of N_2 prior to the CO_2 injection acts as a barrier by creating a thin film layer between CO_2 and CH_4, making it difficult for the carbon dioxide to penetrate and disperse into the methane due to the blanketing nature of nitrogen. This affirmed the use of N_2 for reservoir pressure maintenance for decades. The introduction of N_2 displaces a larger amount of the CH_4 until it reached its breakthrough; this allows most of the CO_2 later injected to be trapped within the rock space without mixing with the nascent CH_4. More so, at the time the CO_2 reaches its breakthrough a substantial volume of CH_4 has been recovered already since the CO_2 will find it difficult to disperse itself into the methane due to the presence of nitrogen gas which acted like a barricaded wall between the CO_2 and CH_4. A decline in the dispersion coefficient was observed as the cushion gas volume increases; thus, less gas miscibility was noticed with higher CO_2 storage compared to the conventional CO_2 flooding. This signifies the feasibility and potential N_2 as a cushioning medium on CH_4 swept recovery efficiency and CO_2 storage for both social and economic benefits.

The variation of effluents against the total injected gases in pore volumes

The breakthrough indicates the first contact point at which the injected gas species (CO_2 and N_2) trespass the length scale of the core sample during the laboratory experimental runs. The later the breakthrough the more the sweep efficiency and invariably the volumes of CO_2 stored. On the other hand, the shorter the breakthrough, the larger the dispersion coefficient; an indication for excessive mixing and product contamination. This results in natural gas production with low calorific value and high purification cost, rendering the process uneconomical. The breakthrough

points were determined from the plots of the concentration profiles against total gas injection as presented in Fig. 9. The effluents mole fraction was measured online using the integrated GC machine as seen from the experimental set-up. Five sets of breakthrough points were measured at 1, 2, 3, and 5 PV of injected gas species. It was observed that there was a delay in the CO_2 breakthrough as the cushion gas volume increases from 1 to 5 PV. This was so because injecting N_2 into the gas-bearing formation can cause a large volume of nascent methane displacement from the reservoir by lowering the partial pressure of CH_4 due to its high conductivity and invariably increase its recovery (Jessen et al. 2008). This accounted for approximately 150% delayed in breakthrough compared to conventional CO_2 injection as evidence in Fig. 9.

The changes in effluent concentration with displacement were ascertained by conventional and gas alternating gas (GAG) displacement simulation (Figs. 10, 11). The N_2 breakthrough occurred when about 6 PV of it been injected into the core sample. This value was roughly 2 times that of the conventional CO_2 injection. The injected pore volume of the CO_2 was earlier detected by the gas chromatography at the same injection temperature and pressure, due to its high diffusion volume. The diffusion volumes of CO_2 and N_2 are 26.9 and 18.5 cm^3, respectively (Fuller et al. 1966). In comparison with conventional N_2 displacement, the breakthrough time of N_2 increases when the cushion gas was employed. The increase was highest at 2 PV cushion gas volume. As expected, more product contamination of N_2 was recorded as the volume of N_2 injected into the system increases. The least contamination was noticed at lower cushion volume with 19% nitrogen contaminants compared to 75% contamination at 5 PV of injected cushion gas. Due to the high cost of natural gas purification, designing an experiment with high product purity is paramount for the economic viability of such a process. Thus, the level of product contamination will be considered in selecting the best and optimum cushion gas volume. Similarly, a prolonged CO_2 breakthrough time was recorded at the highest cushion gas volume (5 PV), this was 5.8 PV more than conventional CO_2 flooding. This also resulted in a higher volume of total injected CO_2 stored due to lower penetration and dispersion coefficient as later present in Table 4. The combined effect for all the runs is presented in Fig. 12. Thus, in turn, the breakthrough of CO_2 can be delayed by increasing N_2 cushion gas volume. Overall, a minimum of 3.2 PV delayed longer than the traditional CO_2 injection was recorded across all the cushion gas volume tested. It evidence that the presence of impurity (N_2) causes large changes in supercritical CO_2 behaviour as reported by several authors (Xidong et al. 2019; Hughes et al. 2012; Janssen et al. 2018; Abba et al. 2018). To reduce the high cost of gas separation, a longer breakthrough with minimum miscibility is preparable for experimental gas injection (Xiangchen et al. 2018). It is worth noting that higher displacement efficiency is obtained at lower cushion volume. The optimization of breakthrough time and displacement efficiency should be expected for the success of the GAG injection process.

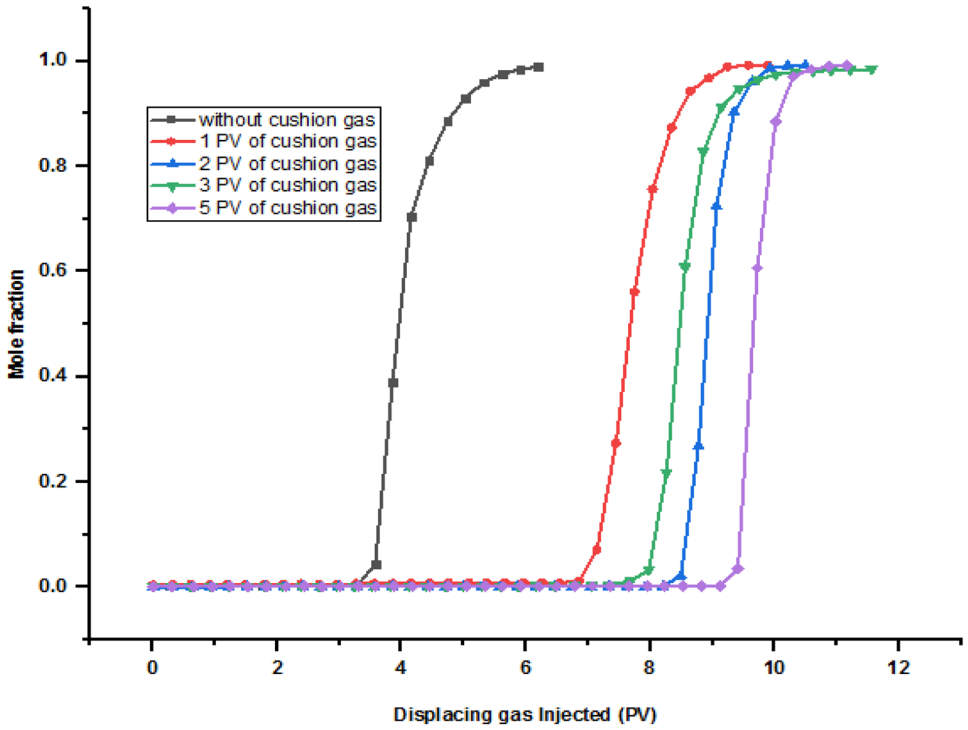

Fig. 9 CO_2 breakthrough time of all the experimental runs

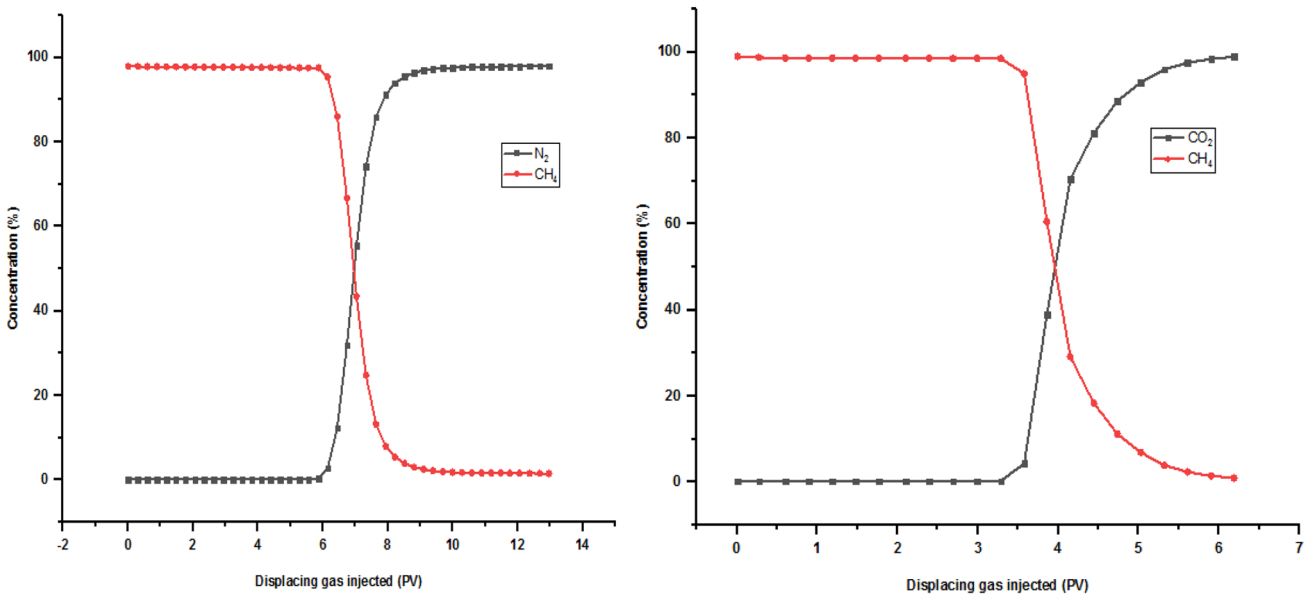

Fig. 10 Conventional N_2 and CO_2 injection effluent concentration profiles

Dispersion coefficient and dispersivity

Dispersion can be defined as an irreversible mixing that exists during miscible displacements reported by Adepoju et al. (2013). This phenomenon occurs mainly due to molecular diffusion and mechanical dispersion as the experiment progress, while the displacing fluids CO_2 and N_2 tend to mix with the displaced CH_4 as shown in the concentration profile plots. The displacement efficiency in miscible flooding is grossly affected by in situ mixing taking place inside the core spaces of the core plug. Also, a transition or mixing zone called 'displacement front' develops when the concentration of methane decreases from > 99% to < 1% as aforementioned in Sect. 4. The dispersion observed reported in Table 5 was used to quantify the nascent mixing as the CO_2 plumes transverses through the porous media. These values were evaluated using empirical evaluation [Eq. (3)] and laboratory experiments by analysing the concentration of CO_2 relative to that of CH_4 in the produced effluent stream with the aid of the GC machine. Several repeated experimental displacement tests were carried out to check for uncertainty and repeatability of the research method and set-up. However, such results were demonstrated in our previous publication. The medium Péclet number (Pe_m) was determined using Eq. (2), in that the characteristic length scale of mixing, d (μm), was obtained from the work of Abba et al. (2019). This value was found to be 57.15 μm for Bandera grey, such value was used in Eq. (2) to determine the dominant phenomenon of displacement mechanism. The Pe_m value was calculated to be 0.02, meaning diffusion is the dominant mechanism since its value is < 0.1 as stated in Sect. 2.1. Also, the dispersivity (α), an empirical property of a porous medium, is responsible for characteristic dispersion of the medium by comparing the components of pore velocity to that of dispersion coefficient. This value was 0.0007 m as reported in our previous work. Thus, in turn, both the medium Péclet number and dispersivity were well within the range obtained by (Abba et al. 2018; Hughes et al. 2012) for consolidated rocks.

Methane recovery

The methane produced was determined based on the total volume and composition of core flooding system effluents recorded by the gas flow meters and gas chromatography. The core flooding experiment was terminated when an insignificance composition (< 0.5%) of CH_4 or (> 99.5%) of CO_2 was noticed from the GC as shown in Fig. 13 with only CO_2 peak noticeable. These volumes are a fraction of the original gas in place (OGIP) in the Bandera grey core plug. The result is presented in Fig. 14. As can be observed, the worst CH_4 recovery was realized when pure CO_2 was injected; this was due to high diffusion volume and low minimum miscibility pressure (MMP) effect as it plumes transverses through the core plug during the displacement process. Considering the GAG injection, the run with 5 PV of cushion gas produced 44.39% CH_4 recovery. This poor sweep efficiency was a result of early N_2 detection by the GC due to the high volume of it injected and demonstrate similar property behaviour with CH_4 as discussed in Sect. 4.1.

Prior to the core flooding experiment, the OGIP of the *Bandera grey* core plug was evaluated using the well-known

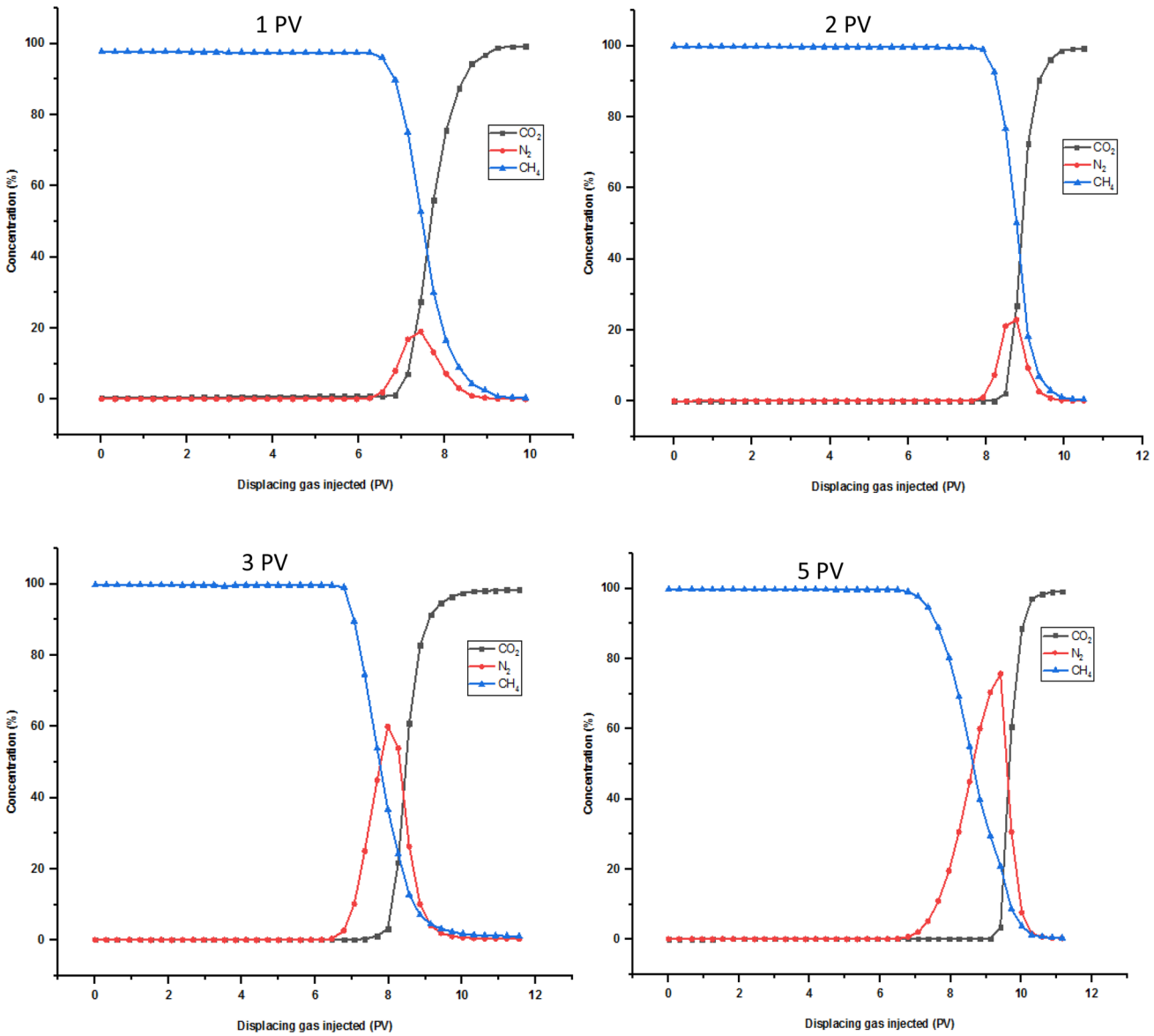

Fig. 11 Effluents concentration profiles with 1, 2, 3, and 5 PV cushion gas

gas reservoir equation [Eq. (8)] as reported by (Abba et al. 2017, 2018).

$$\mathrm{OGIP} = \frac{P_v\left(1 - s_w\right)}{B_g} \tag{8}$$

where G is the original gas in place in scm^3, P_v is the pore volume in cm^3, s_w is the initial water of saturation fraction ($s_w = 0$ for a dry run), and B_g is gas formation volume factor in cm^3/scm^3 for this research. This was then used to determine the percentage of CH_4 recovery as shown in Fig. 14 and Table 3.

Furthermore, the CH_4 recovery was highest for conventional N_2 and 1 PV cushion gas experimental runs. However, not only the 1 PV cushion gas gives high recovery, but also the CH_4 recovered happens to experience the least impurity with 19% N_2 contamination. This signifies the potential application of N_2 gas during the enhanced gas recovery process.

Carbon dioxide injection and storage

In this study, the amount of CO_2 stored during the gas alternating gas injections was evaluated and recorded using Eq. (9) as reported by Xidong et al. (2019).

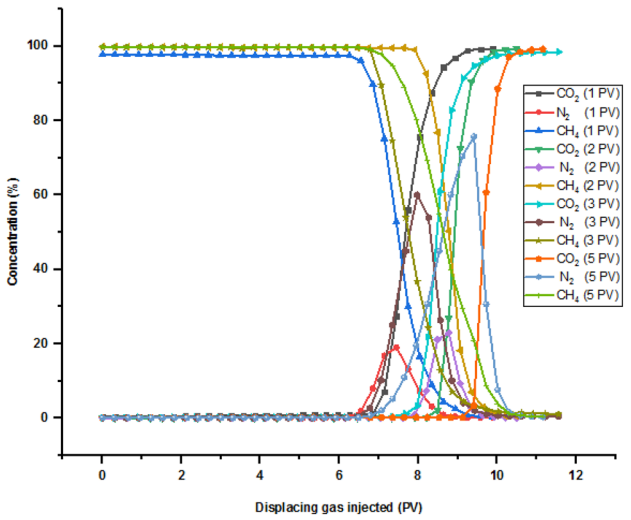

Fig. 12 Concentration profiles of all the runs with cushion gas

$$V_{\text{storage}-CO_2} = V_{t,\text{injected}-CO_2} - F_{\text{outlet}} \int_0^t C_{t,CO_2}\,\mathrm{d}t \tag{9}$$

where $V_{t,\text{injected}-CO_2}$ is the volume of injected CO_2 recorded by the high-pressure syringe pump at time t and C_{t,CO_2} is the CO_2 mole percent in the effluent at time t recorded by the gas chromatography (GC) analyser.

The exit effluents from the core holder were measured using the gas mass flow controller, while the displacing gases were introduced to the system via the ISCO pumps A/B and C/D through cells A and B as presented in Fig. 1. Both pumps were set at a constant flow rate of 0.4 ml/min, and the total injection time was recorded from the online core flooding logging data. For example, to inject 8 cm^3 (1 PV) of the cushion gas (N_2), the ISCO pump A/B was run for 20 min at the set flow rate, i.e. 0.4 cm^3/min × 20 min = 8 cm^3 or 1 PV. Thus, to measure the amount of the rest cushion volumes, the injection period was increased to 40, 60, and 90 min. To evaluate the total CO_2 injected, the total injection time at the end of each experimental test was obtained and the value was multiplied with the known injection rate after taken out the N_2 injection time before introducing the CO_2 into the Bandera grey core sample. For instant, at 1 PV cushion gas, the total injection time was 186.15 as shown in Table 5 in the 'Appendix' section. This means the actual CO_2 injection period is 166.15 min (186.15–20 min). Thus, the total volume of CO_2 injected was 66.46 cm^3 (0.4 cm^3/min × 166.15 min). This value was the same as 8.8 PV of total CO_2 injected. The same procedure is applied to the other experimental runs as shown in Table 4, more so, to evaluate the amount of CH_4 present in the core plug after saturation and before displacing gases injection. The OGIP technique in Eq. (8) was used since the pore volume of the Bandera grey core sample is known. The total volume of

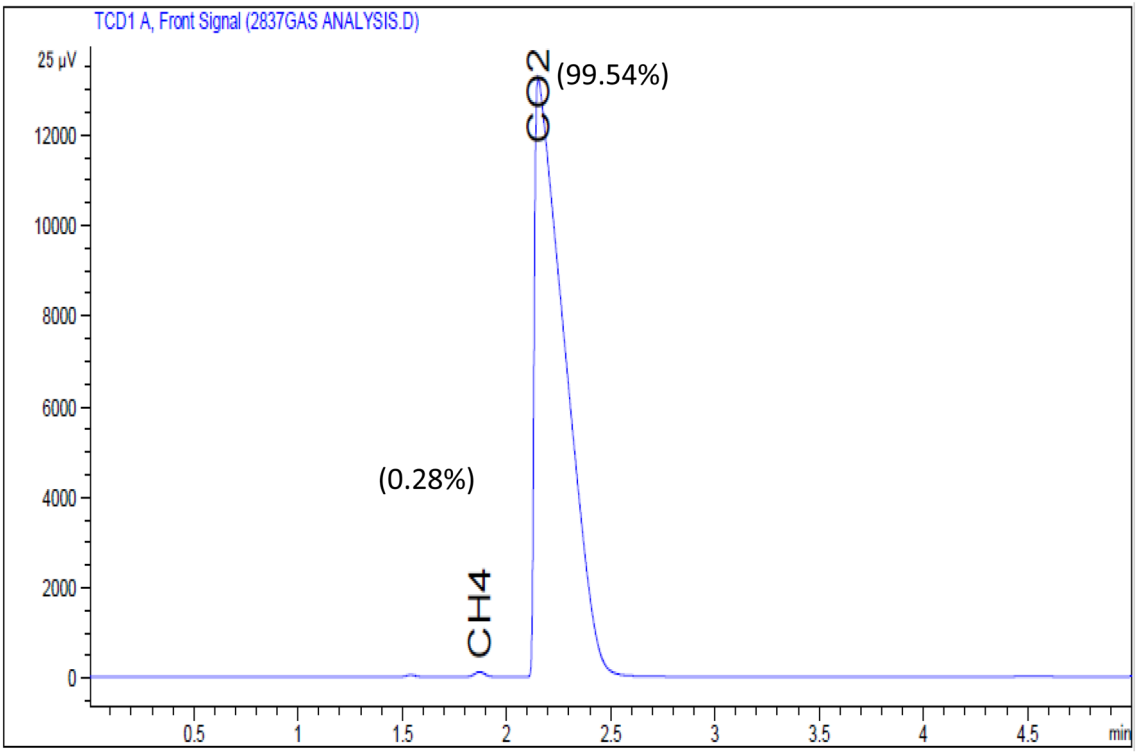

Fig. 13 CO_2 and CH_4 composition recorded by the GC at the termination stage of the core flooding experiment

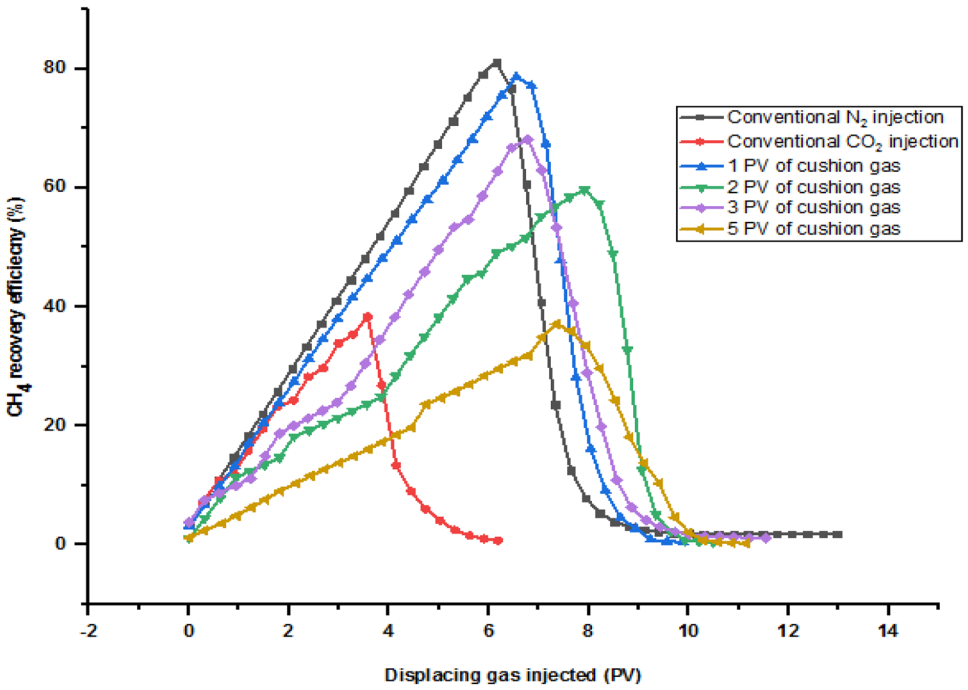

Fig. 14 Graphical representation of percent CH_4 volume produced from all the experimental runs

Table 3 CH_4 recovery factor evaluation for all the injection runs

S/N	Case study	CH_4 In (PV)	CH_4 Produced (PV)	CH_4 Recovery (%)
1	N_2 Injection	115	104.18	90.30
2	CO_2 Injection	115	51.10	44.40
3	1 PV cushion gas	115	102.87	89.17
4	2 PV cushion gas	115	74.77	64.81
5	3 PV cushion gas	115	87.62	75.95
6	5 PV cushion gas	115	51.20	44.39

CH_4 in the core sample was measured to be 115 PV, and is presented in Table 2. The total CO_2 injected stored is presented in Table 4. From Table 4, it is adequate to know that the most significant amount of total CO_2 injected stored of 59.76% was recorded at 2 PV of cushion gas. This was characterized by the large pressure drop (dP) as shown in Fig. 15. The least storage was seen when conventional CO_2 injection was applied. This could be due to the high dispersion coefficient (5.02×10^{-8} m^2/s) obtained during the pure CO_2 injection scenario since this parameter is a key for the economy of the enhanced CH_4 recovery projects (Du et al., 2019). Meanwhile, lower dispersion coefficient weakens the instantaneous mixing effect of CO_2 and CH_4 that inhibits the rapid breakthrough of the injected CO_2. As such, the injection of N_2 as cushion gas can effectively delay or prolonged the breakthrough point, and invariably and sequester more CO_2 over the long run (Xidong et al. 2019).

Table 4 CO_2 produced and stored during EGR for all the injection scenarios

S/N	Case study	CO_2 in (PV)	CO_2 out (PV)	CO_2 stored (PV)	CO_2 stored (%)
1	N_2 injection	0	0	0	0
2	CO_2 injection	6.20	35.63	1.46	23.55
3	1 PV cushion gas	8.80	37.76	3.81	43.30
4	2 PV cushion gas	8.40	25.19	5.02	59.76
5	3 PV cushion gas	8.40	31.93	4.13	49.17
6	5 PV cushion gas	6.40	20.84	3.61	56.41

In consequence, to examine the displacement efficiency in terms of CH_4 recovery and CO_2 sequestration, Tables 3 and 4 were combined to generate Table 5. Looking at the later Table, there was an improvement in both recovery and storage when gas alternating gas injection technique was employed as against that of conventional CO_2 injection. This was so because, as the displacement process proceeds, N_2 does act as a barrier by creating a thin film layer between CO_2 and CH_4, making it difficult for carbon dioxide to penetrate and disperse into the methane due to the blanketing nature of nitrogen. This can be seen, where the least dispersion coefficient of 2.59×10^{-8} m^2/s was recorded at the highest cushion gas volume of 5 PV.

Based on the literature consulted, it is quite difficult to achieve simultaneous CH_4 recovery and CO_2 storage using

Table 5 Efficiency of core flooding process in terms of CH_4 recovery and CO_2 sequestration for all runs

S/N	Case study	Total CO_2 injected stored (%)	CH_4 recovery (%)	Dispersion Coefficient (10^{-8} m^2/s)
1	Conventional N_2 Injection	N/A	90.30	4.40
2	Conventional CO_2 Injection	23.55	44.40	5.02
3	1 PV cushion gas	43.30	89.17	3.59
4	2 PV cushion gas	59.76	64.81	2.78
5	3 PV cushion gas	49.17	75.95	3.27
6	5 PV cushion gas	56.41	44.39	2.59

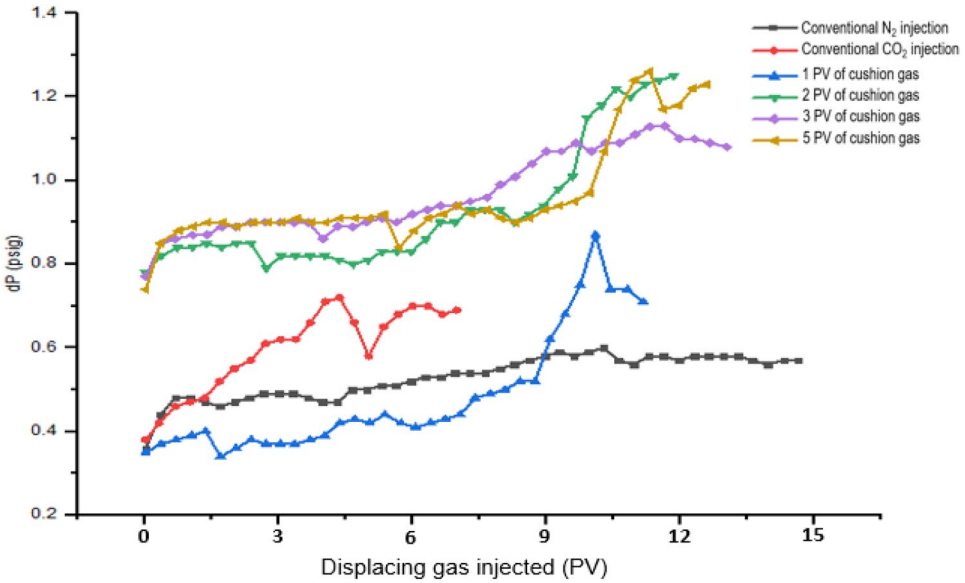

Fig. 15 Differential pressure (dP) changes during the experimental runs with cushion gas compared to conventional injections

conventional injection. For example, Abba et al., (2019) in their work reported high CO_2 storage of 63.13% at 10 wt.% connate water. The same run yielded the poorest CH_4 recovery factor of 16.44% (combined of 79.57%). 'Their reason was due to the restrictive flow when CO_2 traverses the core sample as a result of higher salinity of the connate water sealing off the narrower pore spaces within the pore matrix due to its density'. This means one must be compromised at the expense of the other. However, in this study both were improved compared to conventional single injection. A combination of 124.57% (59.76% CO_2 storage and 64.81% CH_4 recovery) was recorded at 2 PV of cushion gas. The same run gives the second least dispersion coefficient with a prolonged breakthrough point. With the results from the CH_4 recovery efficiency, CO_2 storage, and dispersion coefficient, it is apparent that the best and optimum cushion gas volumes for this study occur at 2 PV.

Conclusion

In this study, the Bandera grey sandstone core plug was used as the standard porous media. An empirical and experimental core flooding runs were carried out to investigate the production of methane and carbon dioxide during EGR displacement scenarios in the presence of N_2 as cushion gas, to register the effects of its existence. A significant recovery and storage of CH_4 and CO_2 were recorded and analysed where the cushion gas volume was 2 PV; this was attributed to the inhibitory flow of the injected CO_2 to disperse itself into the CH_4 and was characterized by low dispersion coefficient. The worst result was obtained at the conventional CO_2 injection scenario. This was due to high CO_2 diffusion volume and low conductivity of CO_2 as it plumes transverses through the core plug during the displacement runs. Methane recovery and carbon dioxide storage can both be influenced by the addition of N_2 as cushion gas prior to CO_2 injection into the reservoir. Thus, in turn, the displacement efficiency of the current research exhibits better results than that of conventional CO_2 injection. However, the presence

of N_2 tends to increase CH_4 recovery by reducing the partial pressure of methane, and at the same time act as a barrier between CO_2 and CH_4 creating a thin barrier making it difficult for early CO_2 breakthroughs as a result of its blanketing effect. This work shows that N_2 as cushion gas influences both CH_4 recovery and CO_2 sequestration. Further work will entail an examination of the effect of connate water salinity on this novel method. Also, the phase behaviour of mixed gases post breakthrough would be investigated.

Acknowledgements The authors wish to acknowledge the Petroleum Technology Development Fund (PTDF) for the studentship and Petroleum and Gas Research Group of the University of Salford, Manchester, UK, for their support.

Appendix

See Tables 6, 7, 8 and 9.

Table 6 Effluent concentrations at 1 PV of cushion gas volume

PVI	CO_2 Conc. (%)	yCO_2	N_2 Conc. (%)	yN_2	CH_4 Conc. (%)	yCH_4
0.01	0.421	0.0042	0.037	0.0004	99.539	0.9954
0.32	0.449	0.0045	0.04	0.0004	99.514	0.9951
0.61	0.465	0.0047	0.042	0.0004	99.493	0.9949
0.92	0.482	0.0048	0.042	0.0004	99.476	0.9948
1.20	0.485	0.0049	0.044	0.0004	99.471	0.9947
1.50	0.501	0.005	0.044	0.0004	99.455	0.9946
1.81	0.501	0.005	0.044	0.0004	99.455	0.9946
2.11	0.510	0.005	0.045	0.0005	99.445	0.9945
2.40	0.560	0.0056	0.045	0.0005	99.395	0.9940
2.68	0.587	0.0059	0.046	0.0005	99.367	0.9937
2.97	0.614	0.0061	0.046	0.0005	99.340	0.9934
3.27	0.615	0.0062	0.046	0.0005	99.339	0.9934
3.57	0.674	0.0067	0.046	0.0005	99.280	0.9928
3.87	0.71	0.0071	0.046	0.0005	99.244	0.9924
4.16	0.739	0.0074	0.046	0.0005	99.215	0.9922
4.46	0.764	0.0076	0.047	0.0005	99.189	0.9919
4.76	0.79	0.0079	0.047	0.0005	99.163	0.9916
5.08	0.819	0.0082	0.047	0.0005	99.134	0.9913
5.37	0.841	0.0084	0.050	0.0005	99.109	0.9911
5.67	0.856	0.0086	0.050	0.0005	99.094	0.9909
5.96	0.856	0.0086	0.051	0.0005	99.093	0.9909
6.26	0.857	0.0086	0.249	0.0025	98.894	0.9889
6.55	0.876	0.0088	1.908	0.0191	97.216	0.9722
6.85	1.166	0.0117	7.961	0.0796	90.873	0.9087
7.14	7.107	0.0711	16.814	0.1681	76.079	0.7608
7.44	27.371	0.2737	19.025	0.1903	53.604	0.536
7.75	56.115	0.5612	13.234	0.1323	30.651	0.3065
8.04	75.681	0.7568	7.141	0.0714	17.178	0.1718
8.34	87.422	0.8742	3.143	0.0314	9.435	0.0944
8.64	94.339	0.9434	0.950	0.0095	4.711	0.0471
8.94	96.827	0.9683	0.408	0.0041	2.765	0.0277
9.24	98.946	0.9895	0.105	0.0011	0.949	0.0095
9.58	99.226	0.9923	0.069	0.0007	0.484	0.0048
9.89	99.317	0.9932	0.060	0.0006	0.404	0.0040

PVI is the total amount of injected gas in pore volumes

Table 7 Effluent concentrations at 2 PV of cushion gas volume

PVI	CO_2 Conc. (%)	yCO_2	N_2 Conc. (%)	yN_2	CH_4 Conc. (%)	yCH_4
0.01	0.018	0.0002	0.027	0.0003	99.955	0.9996
0.32	0.018	0.0002	0.033	0.0003	99.949	0.9995
0.64	0.025	0.0003	0.039	0.0004	99.936	0.9994
0.94	0.030	0.0003	0.042	0.0004	99.928	0.9993
1.22	0.034	0.0003	0.046	0.0005	99.920	0.9992
1.52	0.038	0.0004	0.049	0.0005	99.913	0.9991
1.81	0.040	0.0004	0.051	0.0005	99.909	0.9991
2.11	0.042	0.0004	0.053	0.0005	99.905	0.9991
2.41	0.044	0.0004	0.054	0.0005	99.902	0.9990
2.70	0.046	0.0005	0.055	0.0006	99.899	0.9990
2.98	0.048	0.0005	0.057	0.0006	99.895	0.9990
3.27	0.049	0.0005	0.056	0.0006	99.895	0.9990
3.57	0.051	0.0005	0.057	0.0006	99.892	0.9989
3.85	0.052	0.0005	0.057	0.0006	99.891	0.9989
4.13	0.053	0.0005	0.058	0.0006	99.889	0.9989
4.43	0.056	0.0006	0.059	0.0006	99.885	0.9989
4.71	0.056	0.0006	0.059	0.0006	99.885	0.9989
5.00	0.057	0.0006	0.060	0.0006	99.883	0.9988
5.28	0.057	0.0006	0.061	0.0006	99.882	0.9988
5.58	0.058	0.0006	0.061	0.0006	99.881	0.9988
5.86	0.059	0.0006	0.062	0.0006	99.879	0.9988
6.15	0.060	0.0006	0.062	0.0006	99.878	0.9988
6.46	0.061	0.0006	0.063	0.0006	99.876	0.9988
6.75	0.063	0.0006	0.065	0.0007	99.872	0.9987
7.05	0.064	0.0006	0.066	0.0007	99.870	0.9987
7.33	0.067	0.0007	0.067	0.0007	99.866	0.9987
7.62	0.067	0.0007	0.080	0.0008	99.925	0.9993
7.91	0.069	0.0007	0.918	0.0092	99.013	0.9901
8.21	0.070	0.0007	7.307	0.0731	92.623	0.9262
8.49	2.1450	0.0215	21.087	0.2109	76.768	0.7677
8.77	26.814	0.2681	22.894	0.2289	50.292	0.5029
9.07	72.473	0.7247	9.315	0.0932	18.212	0.1821
9.35	90.375	0.9038	2.685	0.0269	6.940	0.0694
9.64	96.228	0.9623	0.814	0.0081	2.958	0.0296
9.92	98.660	0.9866	0.243	0.0024	1.097	0.0110
10.20	99.152	0.9915	0.152	0.0015	0.696	0.0070
10.50	99.335	0.9934	0.121	0.0012	0.479	0.0048

PVI is the total amount of injected gas in pore volumes

Table 8 Effluent concentrations at 3 PV of cushion gas volume

PVI	CO_2 Conc. (%)	yCO_2	N_2 Conc. (%)	yN_2	CH_4 Conc. (%)	yCH_4
0.01	0.118	0.0012	0.041	0.0004	99.841	0.9984
0.31	0.131	0.0013	0.041	0.0004	99.828	0.9983
0.60	0.137	0.0014	0.413	0.0041	99.815	0.9982
0.94	0.142	0.0014	0.043	0.0004	99.799	0.998
1.23	0.157	0.0016	0.044	0.0004	99.792	0.9979
1.52	0.162	0.0016	0.046	0.0005	99.792	0.9979
1.81	0.162	0.0016	0.046	0.0005	99.789	0.9979
2.09	0.164	0.0016	0.047	0.0005	99.782	0.9978
2.38	0.169	0.0017	0.049	0.0005	99.782	0.9978
2.67	0.169	0.0017	0.049	0.0005	99.777	0.9978
2.97	0.173	0.0017	0.050	0.0005	99.771	0.9977
3.24	0.179	0.0018	0.050	0.0005	99.765	0.9977
3.53	0.185	0.0019	0.050	0.0005	99.763	0.9976
3.82	0.186	0.0019	0.051	0.0005	99.758	0.9976
4.12	0.191	0.0019	0.051	0.0005	99.754	0.9975
4.40	0.193	0.0019	0.053	0.0005	99.749	0.9975
4.71	0.197	0.002	0.054	0.0005	99.748	0.9975
4.99	0.197	0.002	0.055	0.0006	99.745	0.9975
5.30	0.199	0.002	0.056	0.0006	99.741	0.9974
5.59	0.200	0.002	0.059	0.0006	99.741	0.9974
5.88	0.200	0.002	0.059	0.0006	99.737	0.9974
6.17	0.204	0.002	0.059	0.0006	99.716	0.9972
6.45	0.205	0.0021	0.079	0.0008	99.450	0.9945
6.78	0.205	0.0021	2.694	0.0269	97.101	0.9710
7.06	0.205	0.0021	10.214	0.1021	89.581	0.8958
7.35	0.387	0.0039	25.009	0.2501	74.604	0.7460
7.68	1.141	0.0114	44.953	0.4495	53.906	0.5391
7.98	3.269	0.0327	59.989	0.5999	36.742	0.3674
8.26	21.793	0.2179	53.931	0.5393	24.276	0.2428
8.56	60.864	0.6086	26.340	0.2634	12.796	0.1280
8.85	82.816	0.8282	10.089	0.1009	7.095	0.0710
9.14	91.405	0.9141	4.088	0.0409	4.507	0.0451
9.43	94.774	0.9477	2.017	0.0202	3.209	0.0321
9.73	96.533	0.9653	1.111	0.0111	2.356	0.0236
10.00	97.503	0.975	0.727	0.0073	1.770	0.0177
10.30	97.995	0.98	0.559	0.0056	1.446	0.0145
10.60	98.154	0.9815	0.509	0.0051	1.337	0.0134
10.90	98.247	0.9825	0.486	0.0049	1.267	0.0127
11.20	98.378	0.9838	0.455	0.0046	1.167	0.0117
11.60	98.533	0.9853	0.413	0.0041	1.054	0.0105

PVI is the total amount of injected gas in pore volumes

Table 9 Effluent concentrations at 5 PV of cushion gas volume

Time	CO_2 Conc. (%)	yCO_2	N_2 Conc. (%)	yN_2	CH_4 Conc. (%)	yCH_4
0.01	0.047	0.0005	0.039	0.0004	99.914	0.9991
0.31	0.055	0.0006	0.039	0.0004	99.906	0.9991
0.66	0.071	0.0007	0.039	0.0004	99.890	0.9989
0.96	0.085	0.0009	0.039	0.0004	99.876	0.9988
1.25	0.099	0.0010	0.040	0.0004	99.861	0.9986
1.53	0.108	0.0011	0.041	0.0004	99.851	0.9985
1.83	0.115	0.0012	0.041	0.0004	99.844	0.9984
2.15	0.122	0.0012	0.042	0.0004	99.836	0.9984
2.44	0.125	0.0013	0.042	0.0004	99.833	0.9983
2.73	0.128	0.0013	0.043	0.0004	99.829	0.9983
3.02	0.134	0.0013	0.044	0.0004	99.822	0.9982
3.31	0.135	0.0014	0.044	0.0004	99.821	0.9982
3.59	0.136	0.0014	0.044	0.0004	99.820	0.9982
3.88	0.138	0.0014	0.044	0.0004	99.818	0.9982
4.17	0.141	0.0014	0.045	0.0005	99.814	0.9981
4.46	0.143	0.0014	0.046	0.0005	99.811	0.9981
4.74	0.143	0.0014	0.053	0.0005	99.804	0.9980
5.05	0.149	0.0015	0.06	0.0006	99.791	0.9979
5.35	0.151	0.0015	0.06	0.0006	99.789	0.9979
5.63	0.156	0.0016	0.068	0.0007	99.776	0.9978
5.92	0.160	0.0016	0.079	0.0008	99.761	0.9976
6.21	0.164	0.0016	0.094	0.0009	99.742	0.9974
6.50	0.167	0.0017	0.164	0.0016	99.669	0.9967
6.79	0.171	0.0017	0.709	0.0071	99.120	0.9912
7.07	0.174	0.0017	2.063	0.0206	97.763	0.9776
7.36	0.177	0.0018	5.162	0.0516	94.661	0.9466
7.65	0.180	0.0018	10.918	0.1092	88.902	0.889
7.95	0.181	0.0018	19.534	0.1953	80.285	0.8029
8.23	0.186	0.0019	30.643	0.3064	69.171	0.6917
8.53	0.190	0.0019	44.933	0.4493	54.877	0.5488
8.83	0.192	0.0019	60.055	0.6006	39.753	0.3975
9.12	0.200	0.0020	70.416	0.7042	29.384	0.2938
9.41	3.406	0.0341	75.774	0.7577	20.820	0.2082
9.72	60.648	0.6065	30.691	0.3069	8.661	0.0866
10.00	88.588	0.8859	7.601	0.076	3.811	0.0381
10.30	97.136	0.9714	1.593	0.0159	1.271	0.0127
10.60	98.501	0.985	0.716	0.0072	0.783	0.0078
10.90	99.045	0.9905	0.413	0.0041	0.501	0.0050
11.20	99.237	0.9924	0.303	0.0030	0.399	0.0040

PVI is the total amount of injected gas in pore volumes

References

Abba MK, Abbas AJ, Athari A, Martin M, Bello S, Salihu MS, Nasr GG (2019) Solubility trapping as a potential secondary mechanism for CO_2 sequestration during enhanced gas recovery by CO_2 injection in conventional natural gas reservoirs: an experimental approach. J Nat Gas Sci Eng 71:1–12. https://doi.org/10.1016/j.jngse.2019.103002

Abba MK, Abbas AJ, Athari A, Mukhtar A, Nasr GG (2018) Experimental investigation on the impact of connate water salinity on dispersion coefficient in consolidated rocks cores during EGR by CO_2 injection. J Nat Gas Sci Eng 60:190–201. https://doi.org/10.1016/j.jngse.2018.10.007

Abba MK, Abbas AJ, Nasr GG (2017) Enhanced gas recovery by CO_2 injection and sequestration: effect of connate water salinity on displacement efficiency. SPE Abu Dhabi international petroleum exhibition and conference. DOI: 10.2118/188930-MS

Adepoju OO, Lake LW, Johns RT (2013) Investigation of anisotropic mixing in miscible displacements. SPE Reservoir Eval Eng 16:85–96

Al-Abri A, Sidiq H, Amin R (2012) Mobility ratio, relative permeability and sweep efficiency of supercritical CO_2 and methane injection to enhance natural gas and condensate recovery: core flooding experimentation. J Nat Gas Sci Eng 9:166–171. https://doi.org/10.1016/jjngse.2012.05.011

Al-abri A, Sidiq H, Amin R (2009) Enhanced natural gas and condensate recovery by injection of pure $SCCO_2$, pure CH_4 and their mixtures: experimental investigation. In: SPE annual technical conference and exhibition, New Orleans, Louisiana, USA, Vol 4–7, pp 1–13

Al-Hasami A, Ren S, Tohidi B (2005) CO2 injection for enhanced gas recovery and geo-storage: reservoir simulation and economics. In: SPE EUROPEC/EAGE annual conference, 13e16 June. Madrid, Spain, DOI: 10.2118/94129-MS.

de Delgado EIAR (2001) "Dispersion Coefficient Determination for Inert Gas Injection (Nitrogen) in GasLayer". Campinas: Faculty of Mechanical Engineering, State University of Campinas, 2001. Ph.D. thesis. Draft.

Du X, Gu M, Liu Z, Zhao Y, Sun F, Wu T (2019) Enhanced Shale Gas Recovery by the Injections of CO_2, N_2, and CO_2/N_2 Mixture Gases. J Energy Fuels. https://doi.org/10.1021/acs.energyfuels.9b00822

Benson S et al. (2005) Underground geological storage. *Ipcc*, pp.195–276.

Fuller EN, Schettler PD, Giddings JC (1966) New method for prediction of binary gas- 'phase diffusion coefficients. Ind Eng Chem 58:18–27

Ganjdanesh R, Hosseini SA (2017) Geologic Carbon Storage Capacity Estimation Using Enhanced Analytical Simulation Tool (EASiTool). Energy Procedia 114:4690–4696. https://doi.org/10.1016/j.egypro.2017.03.1601

Honari A et al (2013) Dispersion of supercritical CO_2 and CH_4 in consolidated porous media for enhanced gas recovery simulations. Int J Greenhouse Gas Control 19:234–242. https://doi.org/10.1016/j.ijggc.2013.08.016

Honari A et al (2015) Enhanced gas recovery with (CO_2) sequestration: the effect of medium heterogeneity on the dispersion of supercritical CO_2–CH_4. Int J Greenhouse Gas Control 39:39–50

Honari A et al (2016) The impact of residual water on CH_4–CO_2 dispersion in consolidated rock cores. Int J Greenhouse Gas Control 50:100–111. https://doi.org/10.1016/j.ijggc.2016.04.004

Ho C, Webb S (2006) Theory and Applications of Transport in Porous Media.

Hughes TJ et al (2012) CO_2 sequestration for enhanced gas recovery: new measurements of supercritical CO_2–CH_4 dispersion in porous media and a review of recent research. Int J Greenhouse Gas Control 9:457–468. https://doi.org/10.1016/jijggc.2012.05.011

Janssen MTG, Azimi F, Zitha PLJ (2018) Immiscible nitrogen flooding in bentheimer sandstones: comparing gas injection schemes for enhanced oil recovery. Soc Pet Eng. https://doi.org/10.2118/190285-MS

Jessen K, Tang G, Kosvscek AR (2008) Laboratory and simulation investigation of enhanced coalbed methane recovery by gas injection. Transport Porous Medium 73:141–159

Khan C, Amin R, Madden G (2013) Carbon dioxide injection for enhanced gas recovery and storage (reservoir simulation). Egypt J Pet 22(2):225–240

Kalra S, Wu X (2014) CO_2 injection for Enhanced Gas Recovery. SPE Western North American and Rocky Mountain …, (April), pp 16–18. Available at: https://www.onepetro.org/conferencepaper/SPE-169578-MS.

Li X, Kang Y, Zhou L (2018) Investigation of gas displacement efficiency and storage capability for enhanced CH_4 recovery and CO_2 sequestration. J Nat Gas Sci Eng 169:485–493. https://doi.org/10.1016/j.petrol.2018.06.006

Liu S et al (2015) Laboratory experiment of CO_2–CH_4 displacement and dispersion in sandpacks in enhanced gas recovery. J Nat Gas Sci Eng 26:1585–1594. https://doi.org/10.1016/jngse.2015.04.021

Meehl GA, Washington WM, Collins WD, Arblaster JM, Hu A, Buja LE, Strand WG, Teng H (2005) How much more global warming and sea level rise? Science 307:1769–1772

Oldenburg CM, Benson SM (2002) CO_2 injection for enhanced gas production and carbon sequestration. SPE international petroleum conference and exhibition in Mexico. DOI: 10.2118/74367-Ms

Perkins T, Johnston O (1963) A review of diffusion and dispersion in porous media. Soc Petrol Eng J 3(01):70–84. https://doi.org/10.2118/480-PA

Patel MJ, May EF, Johns ML (2016) High-fidelity reservoir simulations of enhanced gas recovery with supercritical CO_2. *Energy,* In Press, pp 548–559. DOI: 10.1016/j.energy.2016.04.120

Pooladi-Darvish M et al. (2008) CO_2 injection for enhanced gas recovery and geological storage of CO_2 in the Long Coulee Glauconite F Pool, Alberta. Proceedings–SPE Annual Technical Conference and Exhibition, 4:2271–2281. Available at: https://www.scopus.com/scopus/inward/record.url?eid=2-s2.0-58849157975&partnerID=40.

Raza A et al (2017) Preliminary assessment of CO_2 injectivity in carbonate storage sites. Petroleum 3(1):144–154. https://doi.org/10.1016/j.petlm.2016.11.008

Rose DA (1973) Some aspects of the hydrodynamic dispersion of solutes in porous materials. J Soil Sci 24(3):284–295

Shtepani E (2006) CO_2 sequestration in depleted gas/condensate reservoirs. Proceedings—SPE Annual Technical Conference and Exhibition.

Sidiq H et al (2011) Super critical CO_2-methane relative permeability investigation. J Petrol Sci Eng 78(3–4):654–663

Sim S et al. (2009) Enhanced gas recovery: effect of reservoir heterogeneity on gas–gas displacement. Canadian international petroleum conference, (June), pp 1–14

Sim SSK et al (2008) SPE 113468 enhanced gas recovery and CO_2 Sequestration by injection of exhaust gases from combustion of bitumen. Changes 1:1–10

Sim SSK et al (2009) Enhanced gas recovery: factors affecting gas-gas displacement efficiency. J Can Pet Technol 48(8):49–55

Turta AT et al. (2007) Basic Investigations on Enhanced Gas Recovery by Gas–Gas Displacement.

Takahashi S, Iwasaki H (1970) The diffusion of gases at high pressures. III. The diffusion of CO_2, in the CO_2–CH_4 system. Bull Chem Res Inst Non-Aqueous Solut Tohoku Univ 20:27–36

Xiangchen L, Yili K, Laicheng Z (2018) Investigation of gas displacement efficiency and storage capability for enhanced CH recovery and CO storage. J Petrol Sci Eng 169:485–493. http://doi.org/10.1016/j.petrol.2018.06.006

Xidong D, Min G, Zhenjian L, Yuan Z, Fulong S, Tengfei W (2019) Enhanced shale gas recovery by the injections of CO, N, and CO /N mixture gases. J Energ Fuel. https://doi.org/10.1021/acs.energyfuels.9b00822

Zhang Y, Liu S, Song Y, Zhao J, Tang L, Xing W, Jian W, Liu Z, Zhan Y (2014) Experimental investigation of CO_2–CH_4 displacement and dispersion in sand pack for enhanced gas recovery. Energy Procedia 61:393–397. https://doi.org/10.1016/j.egypro.2014.11.1133